

## Supporting Information

### **Tuning molecular aggregation to achieve highly bright AIE dots for NIR-II fluorescence imaging and NIR-I photoacoustic imaging**

Yanzi Xu,<sup>[a]</sup> Chunbin Li,<sup>[b]</sup> Ruohan Xu,<sup>[a]</sup> Ning Zhang,<sup>[a]</sup> Zhi Wang,<sup>[a]</sup> Xunan Jing,<sup>[a]</sup> Zhiwei Yang,<sup>[a]</sup> Dongfeng Dang,<sup>[a,\*]</sup> Pengfei Zhang,<sup>[b,\*]</sup> Lingjie Meng<sup>[a,c,\*]</sup>

<sup>[a]</sup> School of Chemistry, MOE Key Laboratory for Non-equilibrium Synthesis and Modulation of Condensed Matter, Xi'an Key Laboratory of Sustainable Energy Material Chemistry, Xi'an Jiao Tong University, Xi'an 710049, P. R. China.

<sup>[b]</sup> Guangdong Key Laboratory of Nanomedicine, CAS Key Laboratory of Health Informatics, Shenzhen Bioactive Materials Engineering Lab for Medicine, Institute of Biomedicine and Biotechnology, Shenzhen Institutes of Advanced Technology, Chinese Academy of Sciences, Shenzhen, 518055, P. R. China.

<sup>[c]</sup> Instrumental analysis center, Xi'an Jiao Tong University, Xi'an, 710049, P. R. China.

E-mail: dongfengdang@xjtu.edu.cn, pf.zhang@siat.ac.cn and menglingjie@xjtu.edu.cn

## Experimental section

### Synthesis

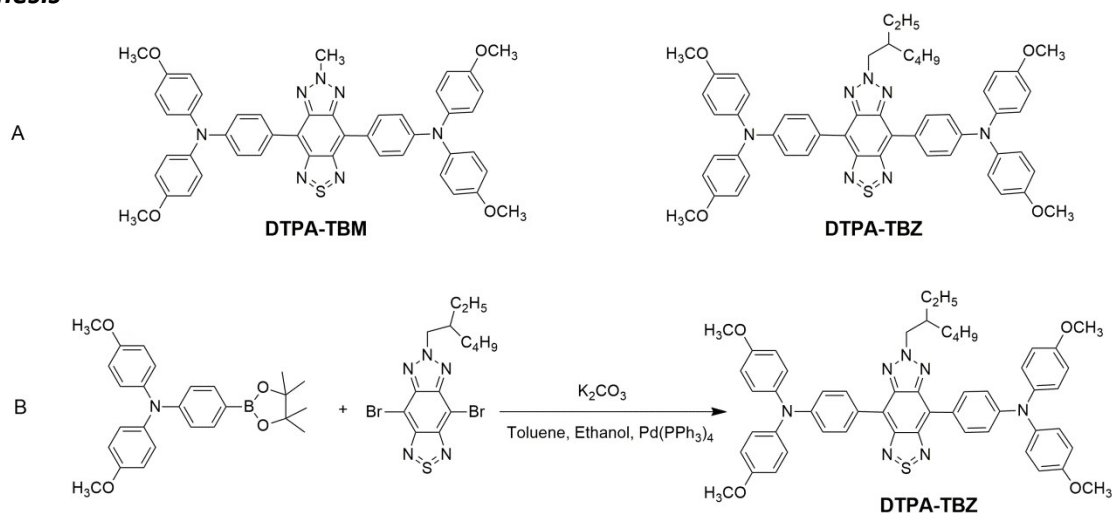


**Figure S1.** Chemical structures of DTPA-TBM and DTPA-TBZ (A); Synthetic route to DTPA-TBZ (B).

### Synthesis of DTPA-TBZ

Tetrakis(triphenylphosphine)palladium [ $Pd(PPh_3)_4$ , 51.70 mg] was added to a mixed solution of N,N-bis(4-methoxyphenyl)-4-(4,4,5,5-tetramethyl-1,3,2-dioxaborolan-2-yl)-benzenamine (925.97 mg, 2.14 mmol) and 4,8-dibromo-6-(2-ethylhexyl)-[1,2,5]thiadiazolo[3,4-f]benzotriazole (400 mg, 0.89 mmol) in toluene (30 mL). Then, anhydrous potassium carbonate ( $K_2CO_3$ ) (2 M, 11.18 mL) and ethanol (10 mL) was also added under nitrogen atmosphere. After stirring at 85 °C for 19 h, the mixture was quenched with water (50 mL) and then was extracted by using dichloromethane (DCM) three times ( $3 \times 70$  mL). After that, the resulted organic solution was dried over anhydrous magnesium sulfate ( $MgSO_4$ ). 30 min later, following by the filtration and removing the solvent, the dark crude product was obtained. After purification with recrystallization by using chloroform as solvent, DTPA-TBZ as deep blue powder was finally obtained with a yield of 78%.  $^1H$ NMR (400 MHz,  $CDCl_3$ ):  $\delta$  8.31 (d,  $J = 8$  Hz, 4H), 7.19 (d,  $J = 12$

Hz, 8H), 7.11 (d,  $J = 12$  Hz, 4H), 6.88 (d,  $J = 12$  Hz, 8H), 4.78 (d,  $J = 4$  Hz, 2H), 3.82 (s, 12H), 1.41-1.36 (m, 6H), 1.29-1.25 (m, 3H), 0.89-0.85 (m, 6H).  $^{13}\text{C}$  NMR (100 MHz,  $\text{CDCl}_3$ )  $\delta$  156.23, 151.47, 148.65, 144.36, 140.36, 131.96, 127.28, 126.76, 119.17, 117.46, 114.74, 61.17, 55.50, 40.50, 30.59, 28.39, 24.01, 22.92, 14.03, 10.53. HRMS (ESI) Calcd for  $\text{C}_{54}\text{H}_{53}\text{N}_7\text{O}_4\text{S}^+$  ( $[\text{M}+\text{H}]^+$ ) 896.3913, Found 896.3920.

#### ***Preparation of DTPA-TBZ-based AIE dots***

To prepare the DTPA-TBZ-based AIE dots, DTPA-TBZ (1.0 mg) and FA-DSPE-PEG2000 (2 mg) were dissolved in THF (1 mL). The solution was quickly injected into a high-speed stirring ultra-pure water (5 mL) for 5 min. Then a microtip probe sonicator (12 W) was used to disperse the organic components in water for 5 minutes. The mixture was then stirred for 10 minutes in an argon atmosphere at room temperature to remove the residual THF. Finally, the dot suspension was filtered through a membrane filter with a diameter of 220 nm and subsequently concentrated to 1.0 mg/mL by using a concentrator (Corning,  $M_w = 30$  K). The nanoparticles were stored in fridge at 4 °C for further use.

#### ***NIR-II fluorescence quantum yield measurement of DTPA-TBZ-based AIE dots***

The fluorescence quantum yield (QY) of DTPA-TBZ-based AIE dots was obtained by using the commercial dye IR-26 as a reference (QY = 0.5%). During the measurement, an initial solution (1 mg/mL) of IR-26 in 1, 2-dichloroethane (DCE) was prepared to produce a series of DCE solutions with absorbance values of  $\sim 0.10$ ,  $\sim 0.08$ ,  $\sim 0.06$ ,  $\sim 0.04$ , and  $\sim 0.02$  in the UV-Vis-NIR range at 808 nm (Figure S8A). The fluorescence emission spectrum was collected by using a 808 nm laser as the excitation source and a 850 nm cut-off filter in the 900-1500 nm region (Figure S8B). Then, identical absorption and emission measurements were performed on the DTPA-TBZ-

based AIE dots in an aqueous solution (Figure S8D-E). Based on the raw data, the integrated fluorescence intensity was plotted as a function of the absorbance at 808 nm (excitation wavelength) and fitted to a linear function (Figure S8C and S8F). According to this method, two slopes were used: one was recorded for the IR-26 DCE reference and the other was obtained from a DTPA-TBZ-based AIE dots sample. The quantum yield of the DTPA-TBZ-based AIE dots in water can be calculated according to the following equation:

$$QY_{sample} = QY_{ref} \times \frac{Slope_{sample}}{Slope_{ref}} \times \left( \frac{\eta_{sample}}{\eta_{ref}} \right)^2$$

Here, the value of  $QY_{ref}$  is 0.5%. The values of  $\eta_{sample}$  and  $\eta_{ref}$  correspond to the refractive index of water and DCE, respectively.

#### ***Photo-stability test of DTPA-TBZ-based AIE dots***

To compare photo-stability of the AIE dots and indocyanine green (ICG), the aqueous solutions containing AIE dots and ICG stored in cuvettes were irradiated with a 808 nm light ( $1 \text{ W cm}^{-2}$ ) for 40 minutes. The cuvettes were imaged using an InGaAs camera with a time interval of 1 minute. The relative PL intensity of the DTPA-TBZ-based dots and ICG were then measured in a selected region of interest (ROI) with a frame size  $50 \text{ pixels} \times 50 \text{ pixels}$  by using Image J for three times.

#### ***Density Functional Theory (DFT) calculation and Molecular dynamics (MD) simulations***

As in previous works,<sup>[1]</sup> the initial configuration of each single molecule (DTPA-TBM and DTPA-TBZ) was optimized based on the density functional theory (DFT) results.<sup>[2]</sup> The geometry optimization and energy calculation were performed at the B3LYP/6-31G(d,p) level.<sup>[3]</sup>

The initial configuration of each aggregate (DTPA-TBM-A and DTPA-TBZ-A) was generated by randomly placing 40 optimized molecules in a  $8.0 \times 8.0 \times 8.0$  nm cubic simulation box.<sup>[4-5]</sup> Each system was then equilibrated during a 25.0 ns molecular dynamics (MD) simulation by using the AMBER suite and the GAFF2 force field. The details of the MD simulation setup are presented in a previous work.<sup>[6]</sup> In brief, each system was solvated with TIP3P waters<sup>[7]</sup> in an isothermal, isobaric ensemble (NPT, T= 298 K and P= 1 atm) with periodic boundary conditions. The MD trajectories were saved every 5.0 ps with an integration time step of 1.0 fs. The Cpptraj module of AmberTools was used to analyze the data.<sup>[8]</sup> The radius of gyration (RoG), the root-mean-square fluctuation (RMSF), and the dihedral angles of each system were monitored to evaluate the structural flexibility.

#### ***Cytotoxicity evaluation of DTPA-TBZ-based AIE dots***

To evaluate the cytotoxicity of DTPA-TBZ dots, LO<sub>2</sub> and 4T1 cells with a concentration of  $5 \times 10^6$  cells in 100  $\mu$ L of medium per well were carefully seeded in fresh 96-well plates. The DTPA-TBZ-based AIE dots with different concentrations (0, 5, 10, 15, 20, and 25  $\mu$ g/mL) were added into the cells. Then, they were co-cultivated for 24 h and 48 h, respectively. After that, the cell WST-1 assay was added to assess the relative cell viability. The cells were washed three times with PBS, and then a fresh aliquot of DMEM (100  $\mu$ L) containing WST-1 solution (10  $\mu$ L) was added in each well. The cells were incubated at 37 °C in 5% of CO<sub>2</sub> for additional 4 h. Their absorbance at 450 nm (reference wavelength) was measured using a microplate reader. The relative viability of the LO<sub>2</sub> and 4T1 cells was calculated by comparing the absorbance by DTPA-TBZ dots-treated cells and the absorbance by the control group (0  $\mu$ g/mL of DTPA-TBZ dots-treated cells).

#### ***Cell imaging***

Dulbecco's modified Eagle's medium (DMEM) were utilized for the culture of HeLa cells, supplemented with fetal bovine serum (FBS, 10%) at 37 °C in a humidified incubator (5% CO<sub>2</sub>). HeLa cells were cultured with DTPA-TBZ-based AIE dots with a concentration of 4 µg/mL and then were washed by phosphate buffered solution (PBS) for three times. Next, the sample was fixed with 10% paraformaldehyde for 10 min. Additionally, DAPI was used to visualize the nuclei, and samples were mounted on slides with glycerol (50%) at the end.

### ***In Vivo fluorescence and PA Imaging***

The BALB/c nude mice were bought from Beijing Vital River Laboratory Animal Technology Co. Ltd. (Beijing, China). The animal experiments were carried out in compliance with the Animal Management Rules of Ministry of Health of the People's Republic of China. The animal treatments were in accordance with the protocols evaluated and approved by the Ethical Committee of the Xi'an Jiao Tong University. The mice model of breast cancer was established by subcutaneously injecting 4T1 tumor cells into the upper right leg of the mice and then waiting for its growth for about a week to make the tumor diameter reach 6-8 mm.

For the fluorescence imaging *in vivo* in the NIR-I window, DTPA-TBZ- based AIE dots were injected into the nude mice *in situ* at the subcutaneous 4T1 tumor (1 mg/mL, 40 µL). The images were taken by using a Xenogen *in vivo* imaging system at different points in time after injection. Then for the fluorescence imaging *in vivo* in the NIR-II window, the mice were intravenously injected in the tail with DTPA-TBZ dots (1 mg/mL, 120 µL) and the images were collected *via* a NIR-OPTICS Series III 900/1700 small animal imaging system (Suzhou NIR-Optics Technology Co., Ltd.) equipped with a 1000 nm long pass filter. The 640 nm and 808 nm lasers (1 W/cm<sup>2</sup>) were used as the light source in the NIR-I and NIR-II fluorescence imaging system.

The signal to background ratios in both cases was processed by using the Image J software by counting six points to obtain an average value. The PA microscopy system was used to collect the images over different time points, where a 790 nm pulsed laser was used in the imaging system.

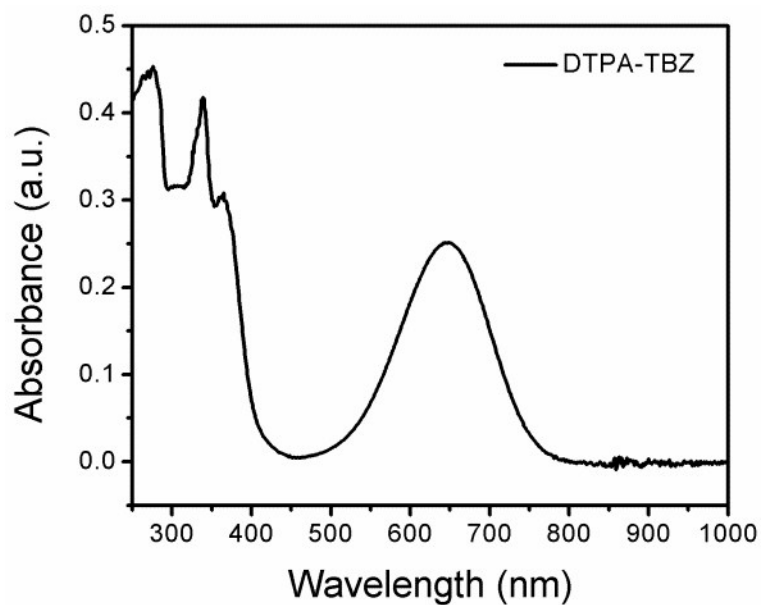


**Figure S2.** UV-Vis absorption spectra of DTPA-TBZ in THF solution ( $[c]= 1\times 10^{-5}$  mol/L).

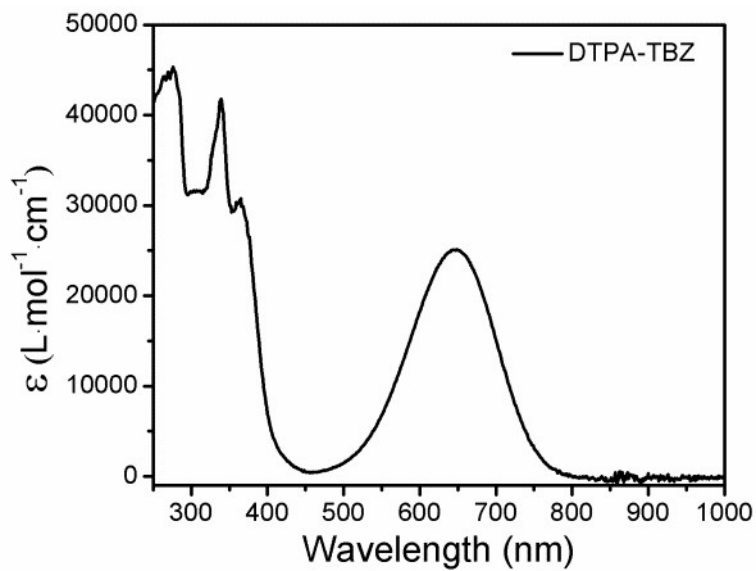


**Figure S3.** Molar absorption coefficient of DTPA-TBZ in dilute THF solution ( $[c]= 1\times 10^{-5}$  mol/L).

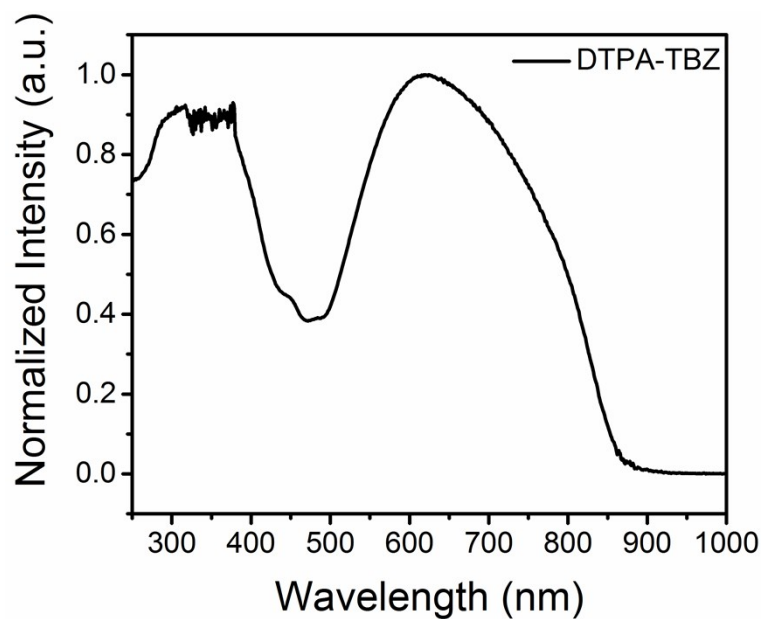


**Figure S4.** UV-Vis absorption of DTPA-TBZ in solid state.

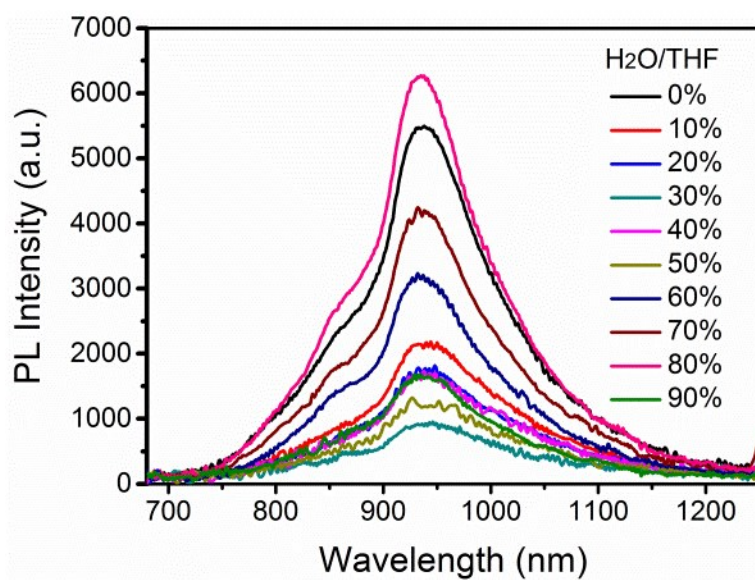


**Figure S5.** Fluorescence intensity of DTPA-TBZ in a THF/water mixture with different water fraction ( $f_w$ ).

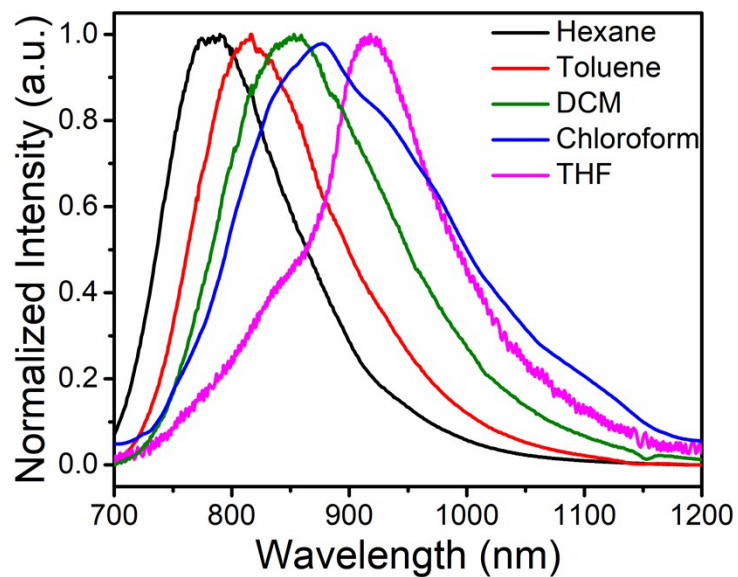


**Figure S6.** Normalized PL spectra of DTPA-TBZ in solvents with varied polarities.

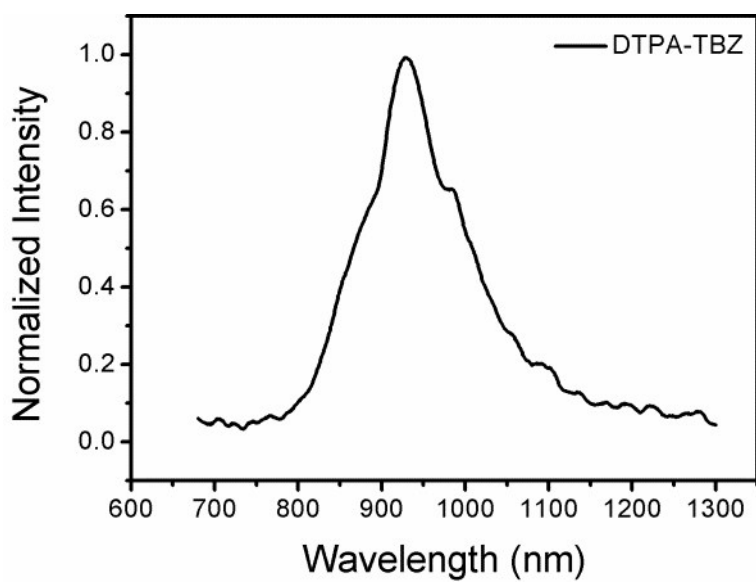


**Figure S7.** PL spectra of DTPA-TBZ in solid state.

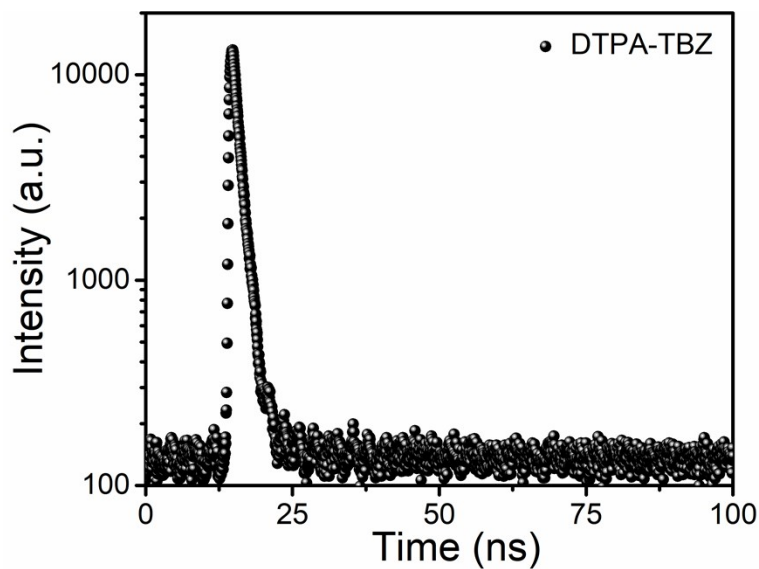


**Figure S8.** Transient decay spectra of DTPA-TBZ in dilute THF solution.

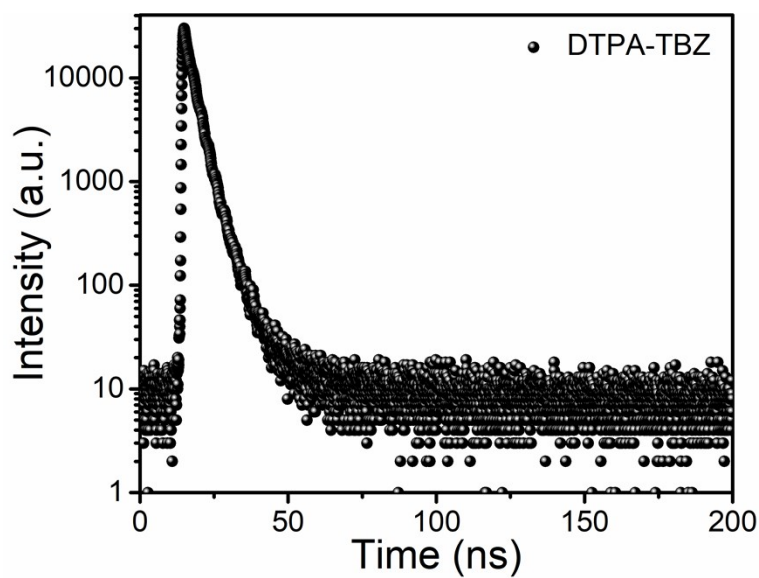


**Figure S9.** Transient decay spectra of DTPA-TBZ in solids.

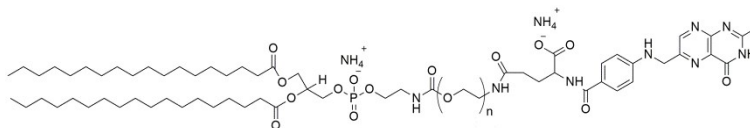


**Figure S10.** Chemical structure of FA-DSPE-PEG ( $M_w = 2000$ ).

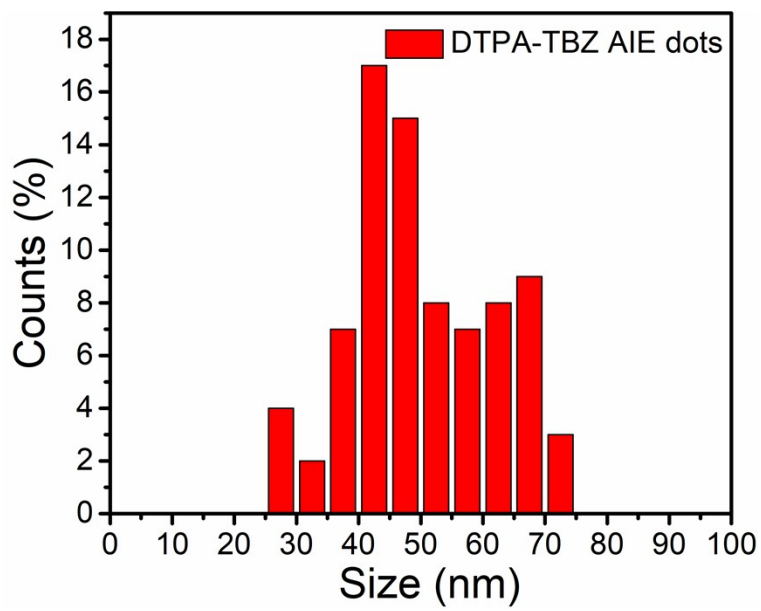


**Figure S11.** Distribution of particle size in prepared AIE dots by TEM analysis.

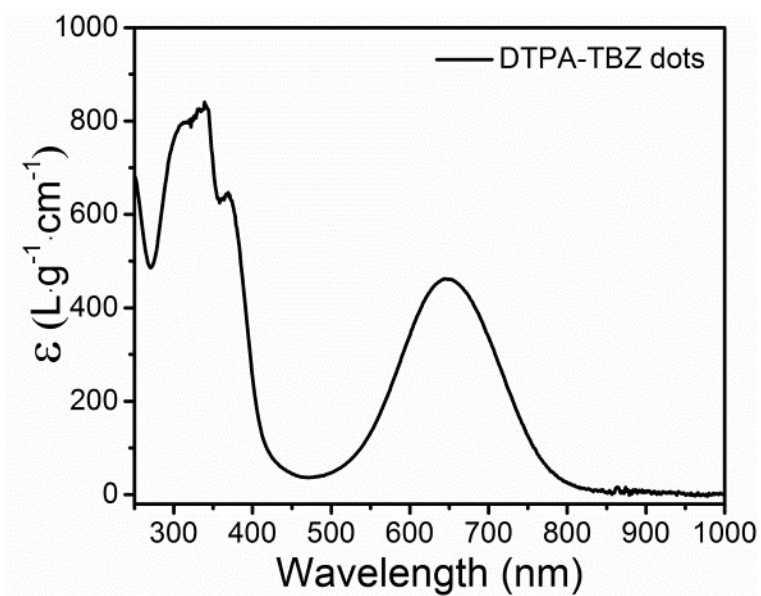


**Figure S12.** Molar extinction coefficient of DTPA-TBZ-based AIE dots in aqueous dispersion.

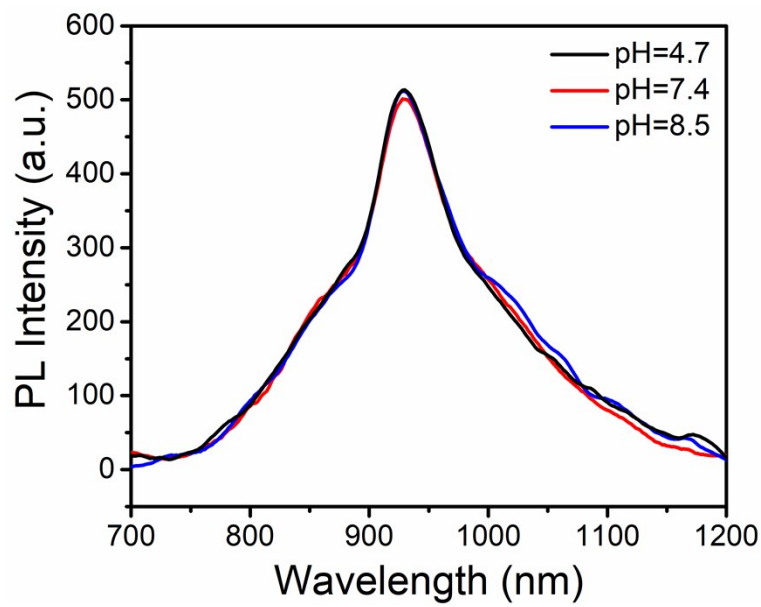


**Figure S13.** PL spectra of AIE dots in aqueous dispersion with various pH values.

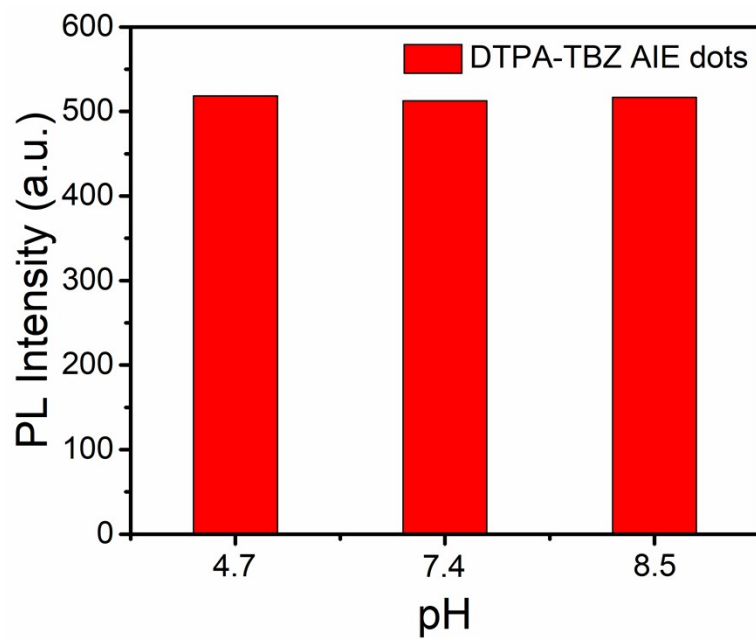


**Figure S14.** Fluorescence intensity of AIE dots in aqueous dispersion with various pH values.

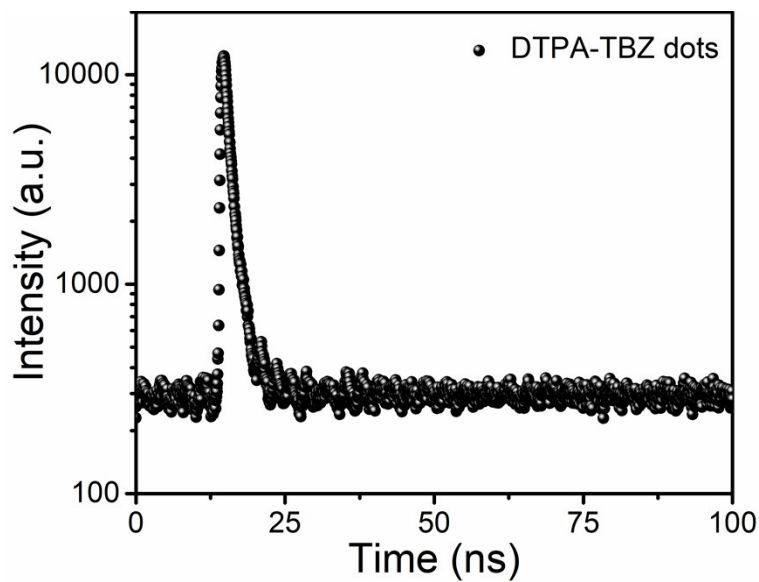


**Figure S15.** Transient decay spectra of AIE dots in aqueous dispersion.

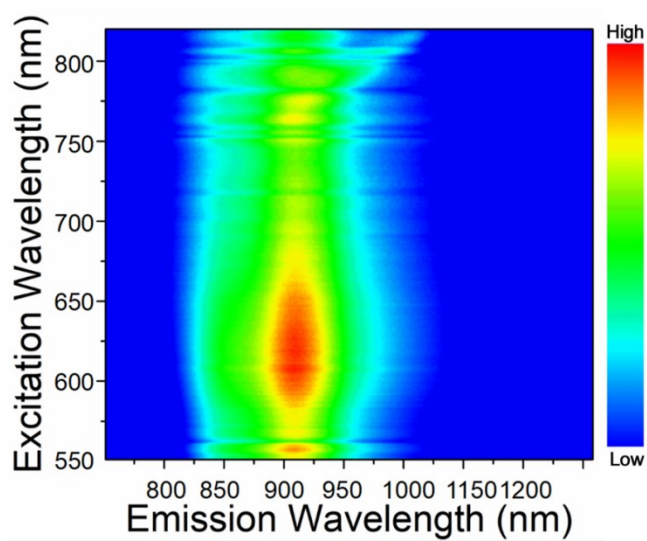


**Figure S16.** PL emission-excitation mapping of DTPA-TBZ-based AIE dots in aqueous dispersion.

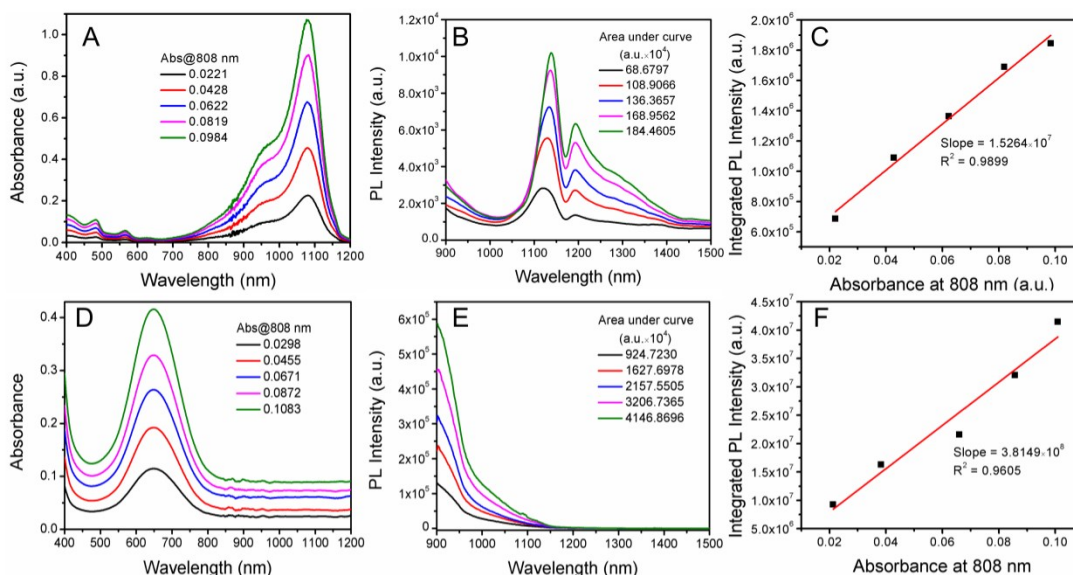


**Figure S17.** UV-Vis-NIR absorption spectra of IR26 in 1,2-dichloroethane (DCE) under different concentrations (A); PL spectra of IR26 in DCE under different concentrations excited by a 808 nm laser (B); Integrated PL intensity plotted as a function of optical density by 808 nm for IR26 based on the measurements in A and B (C); UV-Vis-NIR absorption spectra of DTPA-TBZ-based AIE dots in aqueous solution under different concentrations (D); PL spectra of DTPA-TBZ-based AIE dots under different concentrations excited by a 808 nm laser (E); Integrated PL intensity plotted as a function of optical density by 808 nm for DTPA-TBZ-based AIE dots based on the measurements in D and E (F).

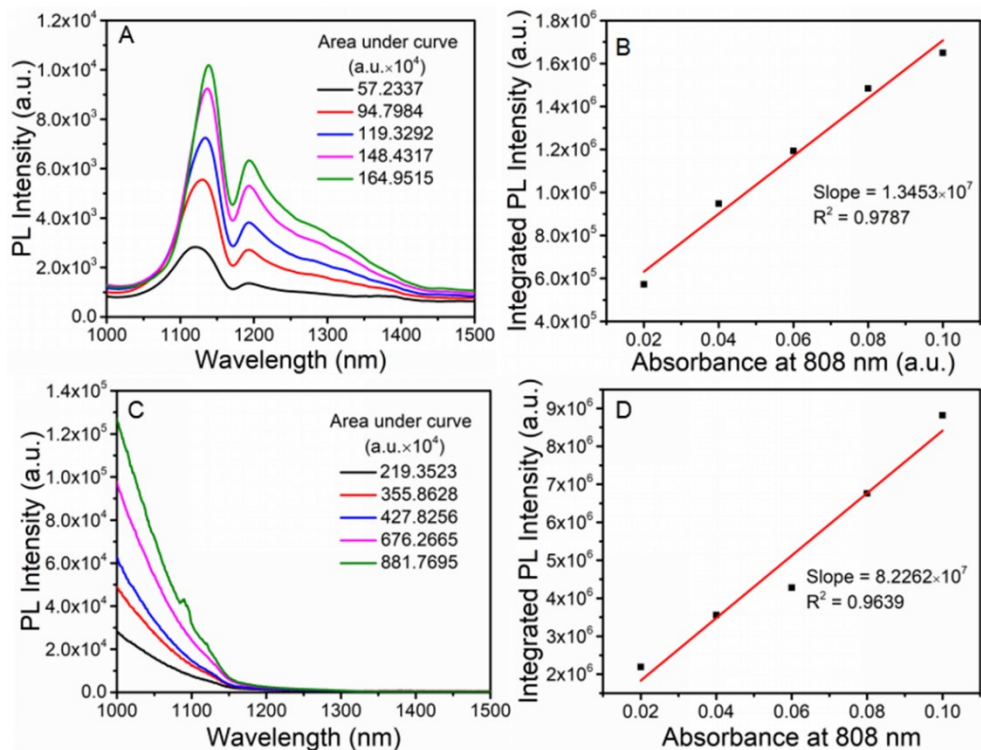


**Figure S18.** PL spectra of IR26 in DCE under different concentrations excited by a 808 nm laser (A); Integrated PL intensity plotted as a function of optical density by 808 nm for IR26 (B); PL spectra of DTPA-TBZ-based AIE dots under different concentrations excited by a 808 nm laser (C); Integrated PL intensity plotted as a function of optical density by 808 nm for DTPA-TBZ-based AIE dots (E).

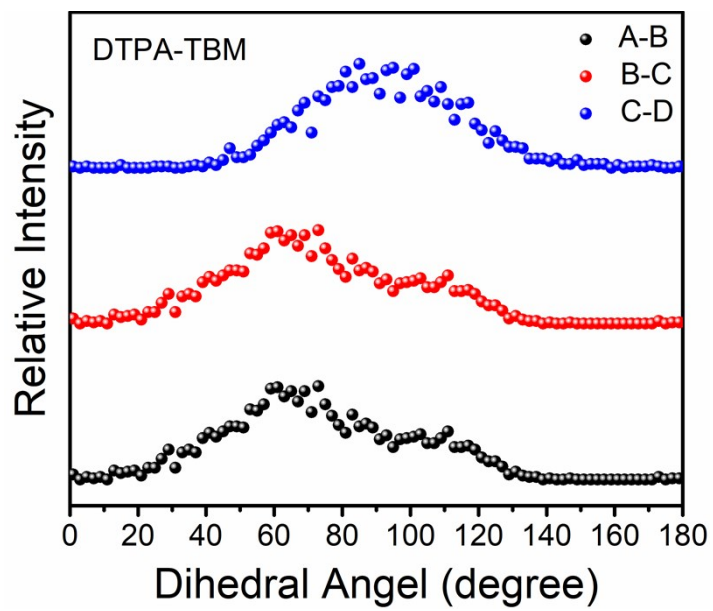


**Figure S19.** Dihedral angle distribution of aromatic rings in DTPA-TBM.

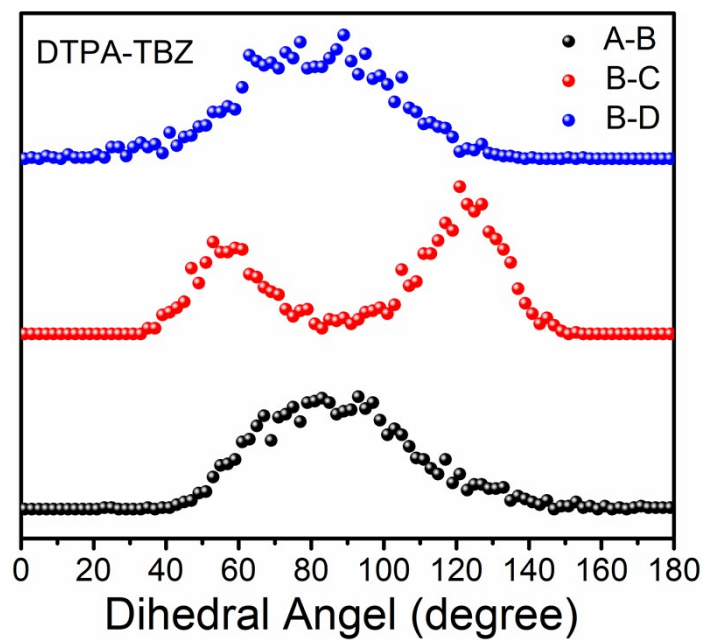


**Figure S20.** Dihedral angle distribution of aromatic rings in DTPA-TBZ.

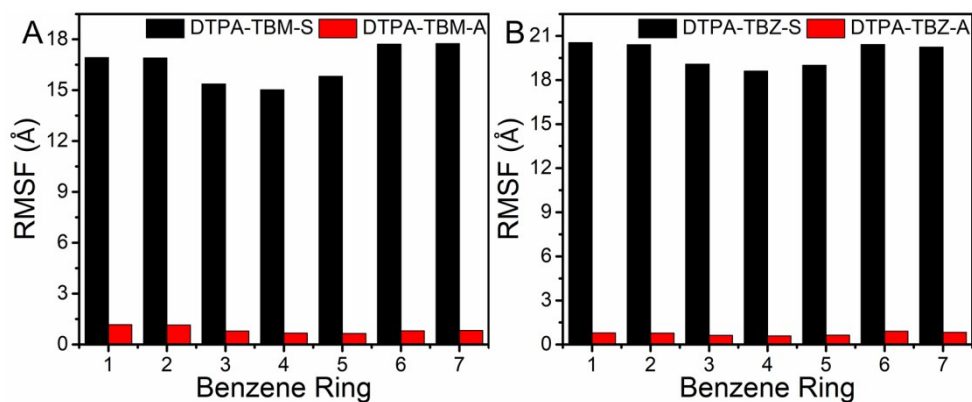


**Figure S21.** Root-mean-square fluctuation (RMSF) values of each phenyl ring over MD simulations for DTPA-TBM (A) and DTPA-TBZ (B) in single molecule and aggregates (single molecule abbreviated as S, aggregate molecules abbreviated as A).

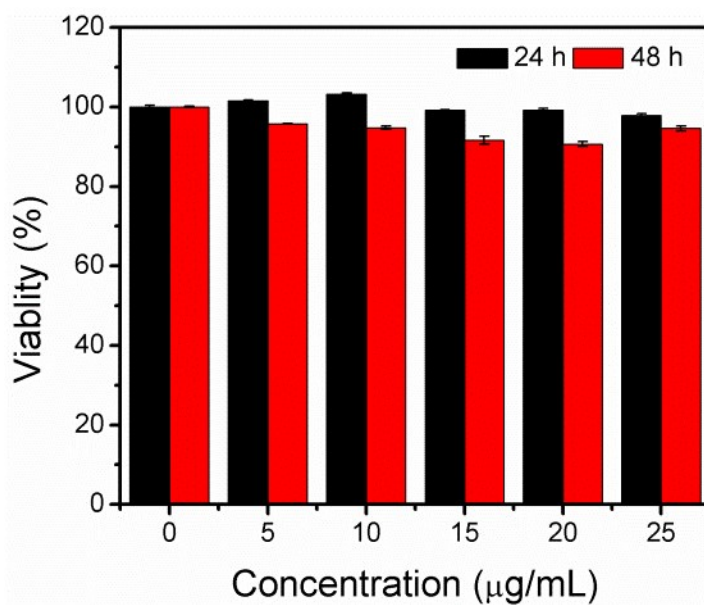


**Figure S22.** Cell viability of LO<sub>2</sub> cells after incubation with DTPA-TBZ-based AIE dots for 24 h and 48 h.

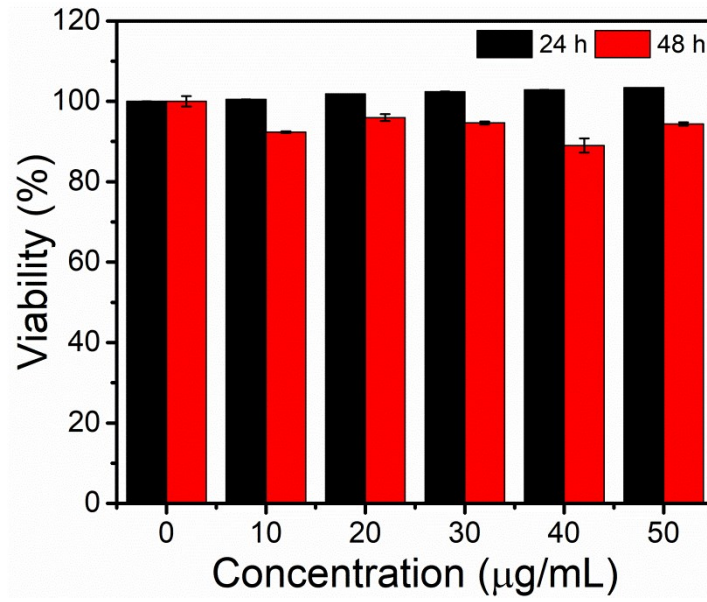


**Figure S23.** Cell viability of 4T1 cells after incubation with DTPA-TBZ-based AIE dots for 24 h and 48 h.

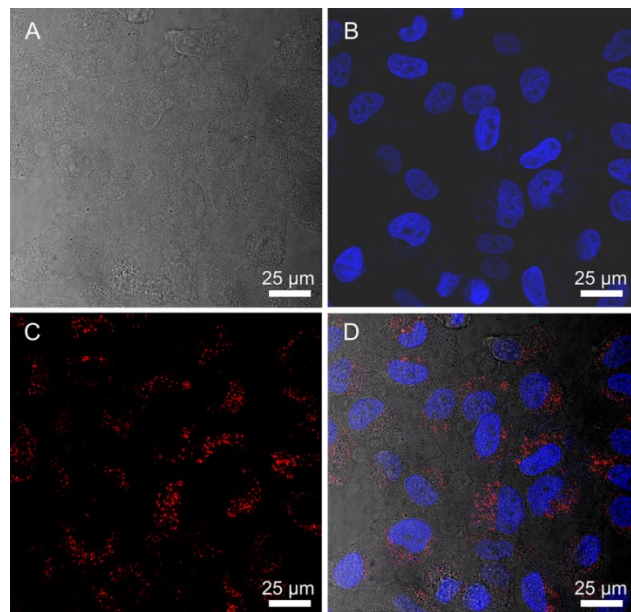


**Figure S24.** CLSM images of HeLa cells in bright field (A), dark field co-stained with DAPI (B), DTPA-TBZ-based AIE dots (C) and their overlapped images (D).

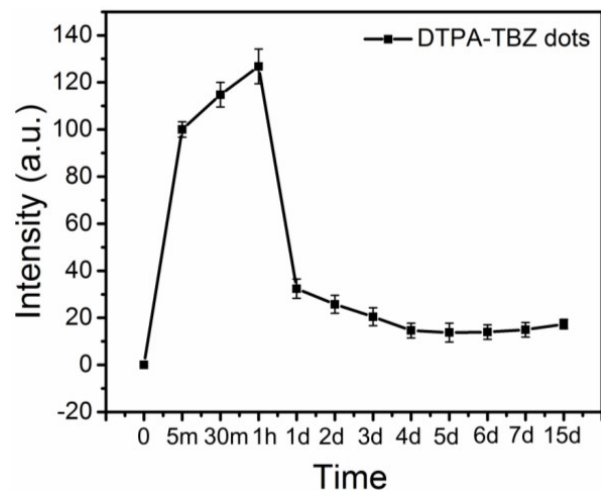


**Figure S25.** Time-dependent fluorescence intensity in NIR-I region for 4T1-tumor in BALB/c nude mice by hypodermic injection of DTPA-TBZ-based AIE dots.

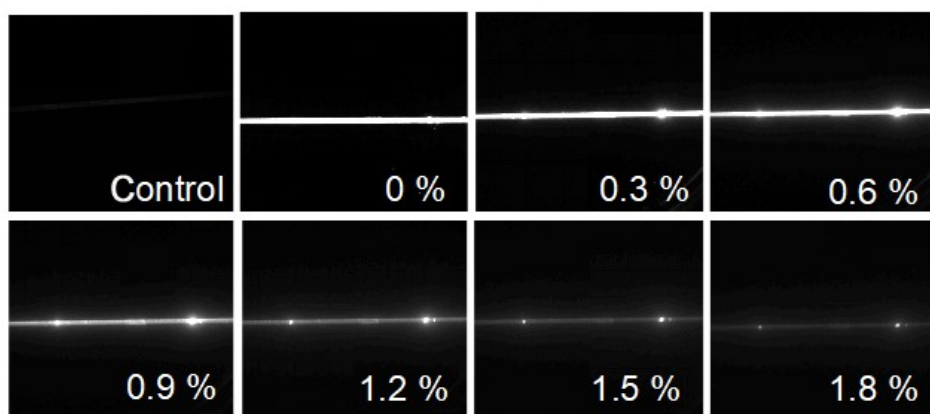


**Figure S26.** Fluorescence images of DTPA-TBZ-based AIE dots (NIR-II, 1200 nm) in tube immersed in intralipid solutions with different concentration at a depth of 0.95 cm excited by a 808 nm diode laser.

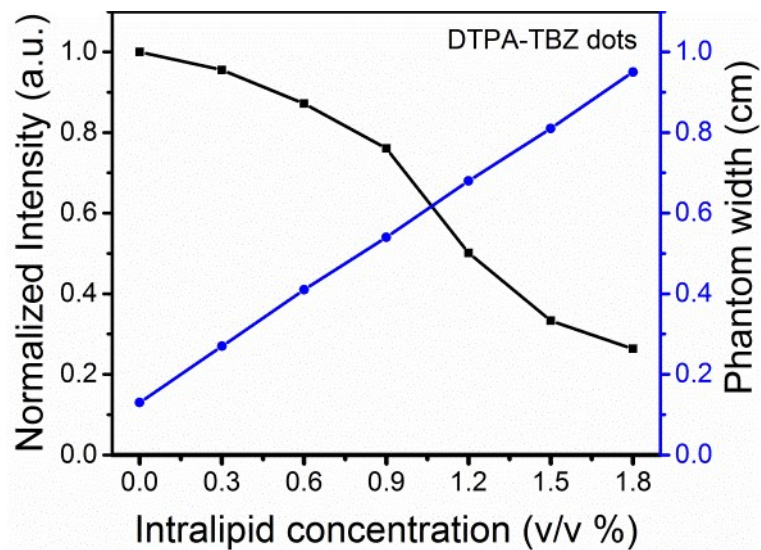


**Figure S27.** Phantom width of capillary images by DTPA-TBZ-based AIE dots corresponding to Figure S17.

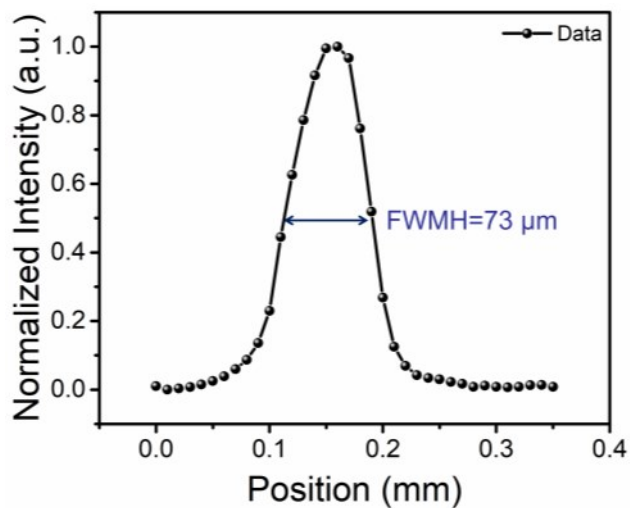


**Figure S28.** The cross-sectional fluorescence intensity profile along the red-dashed line in Figure 4G.

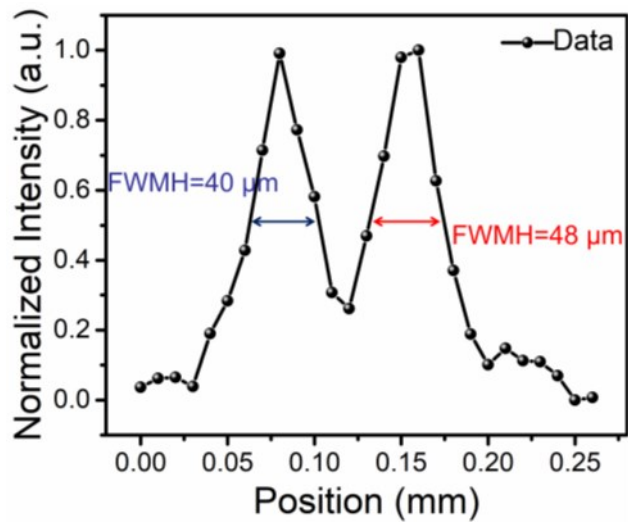


Figure S29. The cross-sectional fluorescence intensity profile along the red-dashed line in Figure 4H.

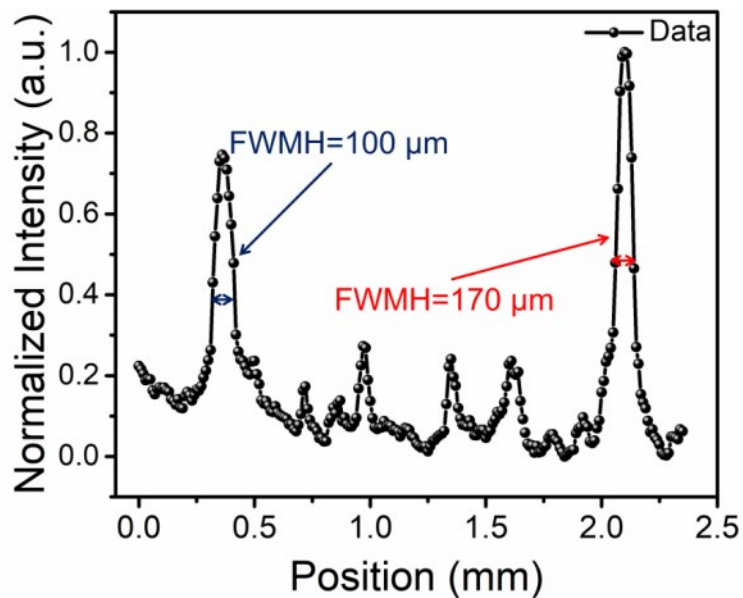
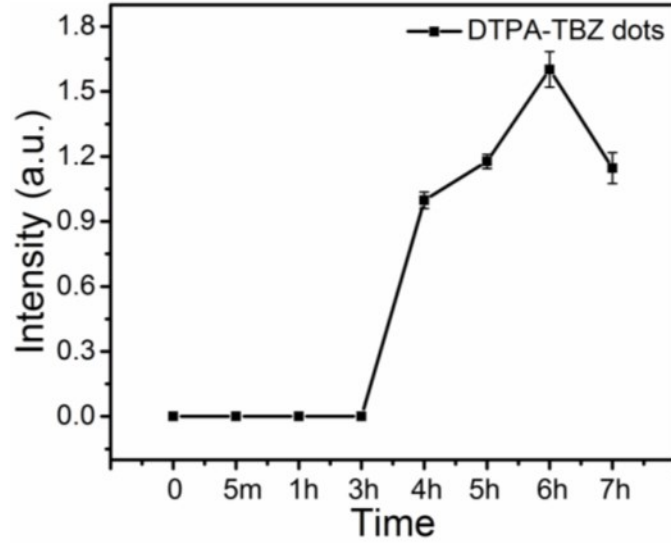
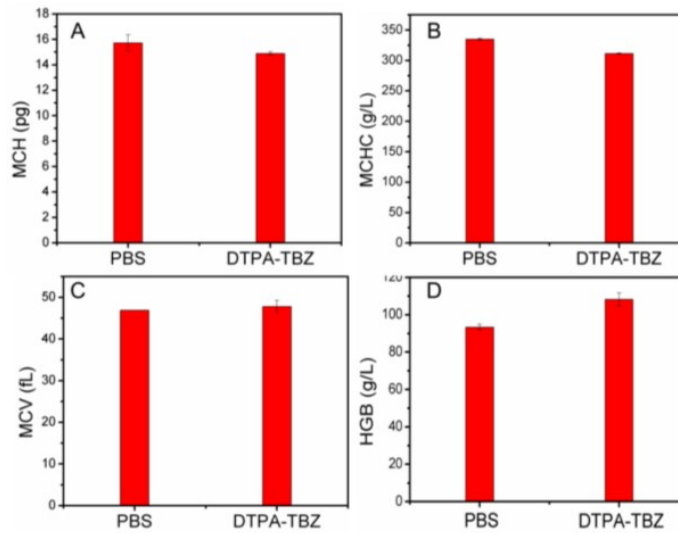


Figure S30. The cross-sectional fluorescence intensity profile along the red-dashed line in Figure 4I.



**Figure S31.** Time-dependent fluorescence intensity in the NIR-II region for 4T1-tumor in BALB/c nude mice by intravenous injection of DTPA-TBZ-based AIE dots.



**Figure S32.** Hematological parameters, including mean corpuscular hemoglobin (MCH), mean corpuscular hemoglobin concentration (MCHC), mean corpuscular volume (MCV) and hemoglobin (HGB), for BALB/c nude mice injected by DTPA-TBZ-based AIE dots and PBS solution.

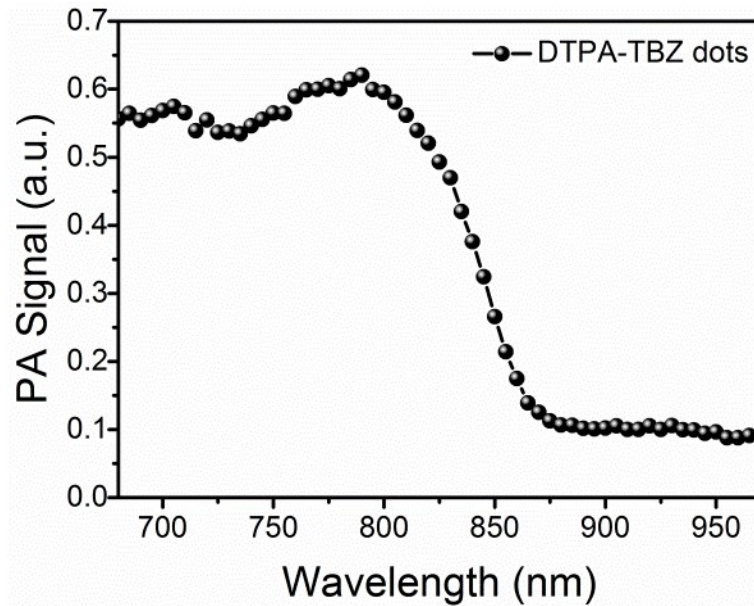


**Figure S33.** PA signal for DTPA-TBZ-based AIE dots in centrifugal tube under different wavelength.

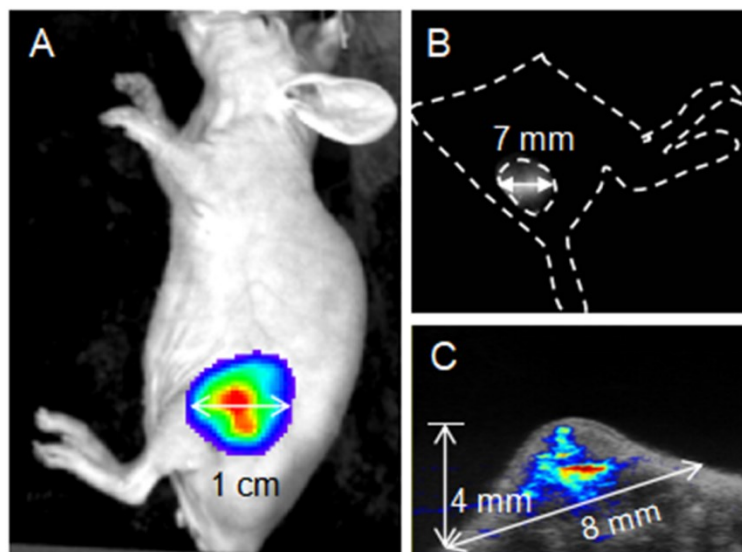
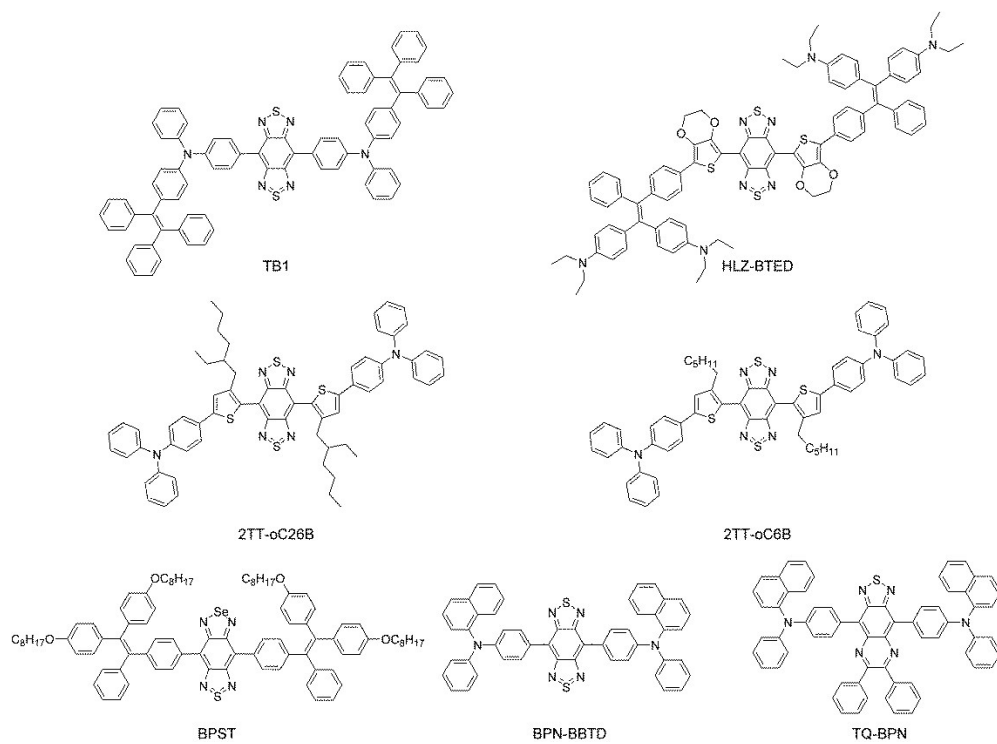


**Figure S34.** Tumor imaging by different imaging mode: NIR-I fluorescence imaging (A); NIR-II fluorescence imaging (B); 3D PA imaging (C).



**Scheme S1.** Chemical structures for some reported organic NIR-II fluorophores.<sup>[9-15]</sup>

**Table S1.** PLQYs of DTPA-TBZ-based AIE dots and some other fluorescence nanoparticles.<sup>[9-17]</sup>

Compounds	PL <sup>[a]</sup>	UV <sup>[b]</sup>	PL <sup>[b]</sup>	PLQYs <sup>[c]</sup>	Reference
TB1	975	800-1200	1050-1500	6.2%	9
BPST	897	600-1100	1000-1500	5.8%	10
HLZ-BTED	1034	700-1000	900-1500	0.18%	11
BPN-BBTD	949	600-900	1000-1600	1.8%	12
TQ-BPN	810	600-850	900-1200	2.8%	13
2TT-oC6B	1030	/	/	11.0%	14
2TT-oC26B	1031	/	1000-1600	11.5%	15
HL3	1050	500-900	1000-1600	11.7%	16
HQL2	1080	500-900	1000-1600	1.19%	17
DTPA-TBZ	929	400-1200	900-1500	11.1%	Our work

<sup>[a]</sup> The PL emission peak for DTPA-TBZ-based AIE dots and other reported fluorescence nanoparticles; <sup>[b]</sup> The UV and PL range for measurement in relative PLQYs; <sup>[c]</sup> PLQYs relative to IR26.

**Table S2.** Photophysical properties of DTPA-TBZ.

Sample	PLQY <sup>[a]</sup> (%)	PLQY <sup>[b]</sup> (%)	$\tau$ <sup>[a]</sup> (ns)	$\tau$ <sup>[b]</sup> (ns)	$k_r$ <sup>[a]</sup> ( $\times 10^7 \text{ S}^{-1}$ )	$k_{nr}$ <sup>[a]</sup> ( $\times 10^7 \text{ S}^{-1}$ )	$k_r$ <sup>[b]</sup> ( $\times 10^7 \text{ S}^{-1}$ )	$k_{nr}$ <sup>[b]</sup> ( $\times 10^7 \text{ S}^{-1}$ )
DTPA-TBZ	3.98	8.98	1.32	3.35	3.02	72.37	2.68	27.17

<sup>[a]</sup> Measured in THF solution; <sup>[b]</sup> Measured in solids. Radiative decay rate in solid state,  $k_r = \text{PLQYs}/\tau$ ; Nonradiative decay rate in solid state,  $k_{nr} = 1/\tau - k_r$ .

**Table S3.** PA properties of DTPA-TBZ-based AIE dots and other fluorescence nanoparticles by using reported organic PA fluorophores.<sup>[9, 16-19]</sup>

Componds	Absorption	Absorption coefficient	PA <sub>ex</sub>	Reference
TB1	500-900 nm	10.2 L·g <sup>-1</sup> ·cm <sup>-1</sup>	740 nm	9
TNMs	600-750 nm	/	710 nm	18
P(DPP-BT/DOX) NPs	620-850 nm	3.05 × 10 <sup>4</sup> L·M <sup>-1</sup> ·cm <sup>-1</sup>	730 nm	19
PBT	750-1064 nm	22.1 L·g <sup>-1</sup> ·cm <sup>-1</sup>	1064 nm	20
PTD	800-1400 nm	48.1 L·g <sup>-1</sup> ·cm <sup>-1</sup>	1160 nm	21
DTPA-TBZ	500-750 nm	462.2 L·g <sup>-1</sup> ·cm <sup>-1</sup>	790 nm	Our work

## Reference

- [1] Dang, D. F.; Zhang, H. K.; Xu, Y. Z.; Xu, R. H.; Wang, Z.; Kwok, R. T. K.; Lam, J. W. Y.; Zhang, L.; Meng, L. J.; Tang, B. Z., *ACS Nano* **2019**, *13*, 11863.
- [2] M. J. Frisch, G. W. T., H. B. Schlegel, G. E. Scuseria, M. A. Robb, J. R. Cheeseman, G. Scalmani, V. Barone, G. A. Petersson, H. Nakatsuji, X. Li, M. Caricato, A. Marenich, J. Bloino, B. G. Janesko, R. Gomperts, B. Mennucci, H. P. Hratchian, J. V. Ortiz, A. F. Izmaylov, J. L. Sonnenberg, D. Williams-Young, F. Ding, F. Lipparini, F. Egidi, J. Goings, B. Peng, A. Petrone, T. Henderson, D. Ranasinghe, V. G. Zakrzewski, J. Gao, N. Rega, G. Zheng, W. Liang, M. Hada, M. Ehara, K. Toyota, R. Fukuda, J. Hasegawa, M. Ishida, T. Nakajima, Y. Honda, O. Kitao, H. Nakai, T. Vreven, K. Throssell, J. A. Montgomery, Jr., J. E. Peralta, F. Ogliaro, M. Bearpark, J. J. Heyd, E. Brothers, K. N. Kudin, V. N. Staroverov, T. Keith, R. Kobayashi, J. Normand, K. Raghavachari, A. Rendell, J. C. Burant, S. S. Iyengar, J. Tomasi, M. Cossi, J. M. Millam, M. Klene, C. Adamo, R. Cammi, J. W. Ochterski, R. L. Martin, K. Morokuma, O. Farkas, J. B. Foresman, and D. J. Fox *Gaussian 09, Revision A.02*; Gaussian, Inc.: Wallingford CT, 2016., 2016.
- [3] Yang, Z. W.; Yang, G.; Zu, Y. G.; Fu, Y. J.; Zhou, L. J., *Physical Chemistry Chemical Physics* **2009**, *11*, 10035.
- [4] Martinez, L.; Andrade, R.; Birgin, E. G.; Martinez, J. M., *J. Comput. Chem.* **2009**, *30*, 2157.
- [5] Wang, D.; Lee, M. M. S.; Xu, W. H.; Shan, G. G.; Zheng, X. Y.; Kwok, R. T. K.; Lam, J. W. Y.; Hu, X. L.; Tang, B. Z., *Angew Chem. Int. Edit.* **2019**, *58*, 5628.
- [6] Dang, D.; Wang, X.; Wang, D.; Yang, Z.; Hao, D.; Xu, Y.; Zhang, S.; Meng, L., *ACS Appl. Nano Mater.* **2018**, *1*, 2324.

- [7] Jorgensen, W. L.; Chandrasekhar, J.; Madura, J. D.; Impey, R. W.; Klein, M. L., *J. Chem. Phys.* **1983**, *79*, 926.
- [8] Roe, D. R.; Cheatham, T. E., III, *J. Chem. Theory Comput.* **2013**, *9*, 3084.
- [9] Zonghai Sheng, Bing Guo, Dehong Hu, Shidang Xu, Wenbo Wu, Weng Heng Liew, Kui Yao, Jingying Jiang, Chengbo Liu, Hairong Zheng, Bin Liu. *Adv. Mater.* **2018**, *30*, 1800766.
- [10] Wei Wu, Yanqing Yang, Yang Yang, Yuming Yang, Kaiyuan Zhang, Li Guo, Hongfei Ge, Xiaowei Chen, Jie Liu, Hua Feng. *Small* **2019**, *15*, 1805549
- [11] Jiacheng Lin, Xiaodong Zeng, Yuling Xiao, Lin Tang, Jinxia Nong, Yufang Liu, Hui Zhou, Bingbing Ding, Fuchun Xu, Hanxing Tong, Zixin Deng, Xuechuan Hong. *Chem. Sci.* **2019**, *10*, 1219.
- [12] Nuernisha Alifu, Abudureheman Zebibula, Ji Qi, Hequn Zhang, Chaowei Sun, Xiaoming Yu, Dingwei Xue, Jacky W. Y. Lam, Gonghui Li, Jun Qian, Ben Zhong Tang. *ACS Nano* **2018**, *12*, 11282.
- [13] Ji Qi, Chaowei Sun, Abudureheman Zebibula, Hequn Zhang, Ryan T. K. Kwok, Xinyuan Zhao, Wang Xi, Jacky W. Y. Lam, Jun Qian, Ben Zhong Tang. *Adv. Mater.* **2018**, *30*, 1706856.
- [14] Shunjie Liu, Chao Chen, Yuanyuan Li, Haoke Zhang, Junkai Liu, Ran Wang, Sherman T. H. Wong, Jacky W. Y. Lam, Dan Ding, Ben Zhong Tang. *Adv. Funct. Mater.* **2019**, *30*, 1908125.
- [15] Yuanyuan Li, Zhaochong Cai, Shunjie Liu, Haoke Zhang, Sherman T.H. Wong, Jacky W.Y. Lam, Ryan T.K. Kwok, Jun Qian, Ben Zhong Tang. *Nat. Commun.* **2020**, *11*, 1255.
- [16] Yang Li, Yufang Liu, Qianqian Li, Xiaodong Zeng, Tian Tian, Wenyi Zhou, Yan Cui, Xikun Wang, Xiaoding Cheng, Qihang Ding, Xiaofei Wang, Junzhu Wu, Hai Deng, Yanqin Li, Xianli Meng, Zixin Deng, Xuechuan Hong, Yuling Xiao. *Chem. Sci.* **2020**, *11*, 2621.

- [17] Qianqian Li, Qihang Ding, Yang Li, Xiaodong Zeng, Yishen Liu, Siyu Lu, Hui Zhou, Xiaofei Wang, Junzhu Wu, Xianli Meng, Zixin Deng, Yuling Xiao. *Chem. Commun.* **2020**, *56*, 3289.
- [18] Shaobo Zhang, Weisheng Guo, Jie Wei, Chan Li, Xing-Jie Liang, Meizhen Yin. *ACS Nano* **2017**, *11*, 3797–3805.
- [19] Qi Wang, Yeneng Dai, Jingzeng Xu, Jie Cai, Xinrui Niu, Lei Zhang, Runfeng Chen, Qingming Shen, Wei Huang, Quli Fan. *Adv. Funct. Mater.* **2019**, 1901480.
- [20] Bing Guo, Zhe Feng, Dehong Hu, Shidang Xu, Eshu Middha, Yutong Pan, Chengbo Liu, Hairong Zheng, Jun Qian, Zonghai Sheng, Bin Liu. *Adv. Mater.* **2019**, *31*, 1902504.
- [21] Bing Guo, Jingqin Chen, Ningbo Chen, Eshu Middha, Shidang Xu, Yutong Pan, Min Wu, Ke Li, Chengbo Liu, Bin Liu. *Adv. Mater.* **2019**, *31*, 1808355.

# NMR and Mass spectrum

